Electronic Research Archive

https://www.aimspress.com/journal/era

ERA, 33(3): 1589–1609.
DOI: 10.3934/era.2025075
Received: 20 January 2025
Revised: 09 March 2025
Accepted: 14 March 2025
Published: 19 March 2025

Research article

A nonlinear correction finite volume scheme preserving maximum principle for diffusion equations with anisotropic and discontinuous coefficient

Yao Yu[1,*] **and Guanyu Xue**[2]

[1] College of Mathematics and System Science, Shandong University of Science and Technology, Qingdao 266590, China

[2] School of Mathematics and Information Sciences, Yantai University, Yantai 264005, China

* **Correspondence:** Email: yuyao0608@163.com.

Abstract: A nonlinear correction finite volume scheme preserving the discrete maximum principle (DMP) was presented to solve diffusion equations with anisotropic and discontinuous coefficients. It is well-known that existing cell-centered finite volume schemes for the diffusion problem with the general discontinuous coefficient often impose severe restrictions on the mesh-cell geometry to maintain the DMP. We proposed a nonlinear method for modifying the flux to obtain a new scheme which eliminated the requirement for nonnegative interpolation coefficients at the midpoint of cell-edge unknowns while still preserving the DMP. That is, our new scheme satisfied the DMP unconditionally and can be applied to the diffusion problem with the discontinuous coefficient on arbitrary distorted meshes. We then provided a priori estimation under a coercivity assumption and proved that the scheme satisfied the DMP. Numerical results were presented to demonstrate that our scheme can handle diffusion equations with anisotropic and discontinuous coefficients, satisfied the DMP, and, in some cases, outperformed existing schemes which preserved the DMP in terms of accuracy.

Keywords: maximum principle; nonlinear correction; finite volume scheme; discontinuous coefficient; diffusion equations

1. Introduction

A discrete scheme that satisfies fundamental properties such as conservation, positivity, and the discrete maximum principle (DMP) for the diffusion equations is of great significance. The finite volume framework can ensure local conservation of mass, an essential physical property, and is a commonly used method in constructing the discretization system (see [1–4]). There is a lot of research on the monotonicity of scheme, as it guarantees the positivity of the approximate solution (see [5–10]). However, a monotone scheme can only maintain the lower bound and cannot simultaneously

keep the upper bound. A discrete system preserving the DMP can ensure that there are no spurious oscillations in the numerical solutions and can preserve physical bounds. Therefore, researchers have recently turned to constructing schemes that preserve the DMP (see [11–15]). A scheme having a specific structure ensures the DMP is developed in [16], which provides some theoretical analysis under the coercivity assumption. In [17], a nonlinear finite volume scheme preserving the DMP for the anisotropic diffusion equations on distorted meshes is presented. They give a proof of the coercivity of the scheme under some constraints on cell deformation and the diffusion coefficient.

It is challenging to design a precise and dependable scheme on distorted meshes for the diffusion problem with anisotropic and discontinuous coefficients to satisfy the DMP. As is well-known, the existing cell-centered finite volume schemes for the diffusion problem with general discontinuous coefficients on general meshes cannot unconditionally satisfy the DMP. The validity of the DMP for continuous piecewise linear finite element approximations for the Poisson equation with the Dirichlet boundary condition is verified in [18]. A nonlinear stabilized Galerkin approximation of the Laplace operator, which preserves the DMP on arbitrary meshes and in arbitrary space dimension without the help of the well-known acute condition or generalizations thereof, was derived in [19]. A mesh condition is developed for linear finite element approximation of the anisotropic diffusion–convection–reaction problem to satisfy the DMP in [20]. A weak Galerkin discrete scheme preserving the DMP for the boundary value problem of a general anisotropic diffusion problem is created in [21]. From all of the above methods, we find that there are invariably certain restrictions on the geometry of mesh-cell or the location of discontinuity in order to preserve the DMP. Desirably, our new scheme can satisfy the DMP unconditionally.

For constructing a scheme satisfying monotone or the DMP, many researchers take a measure of making a correction on flux. In [22], a nonlinear method to correct a general finite volume scheme for the anisotropic diffusion problem, which preserves the DMP, was presented. A monotonicity correction was applied to second-order element finite volume methods, obtaining a second-order monotone finite volume scheme for the anisotropic diffusion problem in [23]. In [24], a new nonlinear method is constructed to preserve the DMP for the diffusion problem with the heterogeneous anisotropic coefficient. Following this idea, we propose a nonlinear correction for the finite volume method to obtain a scheme that preserves the DMP, where the interpolation coefficients of the cell-edge unknowns are not required to be nonnegative. This is an advantage of our scheme.

In this paper, we propose a new nonlinear correction finite volume scheme to preserve the DMP for diffusion equations with anisotropic and discontinuous coefficients. First, two linear and nonconservative fluxes are given on two sides of the cell-edge, respectively. Meanwhile, cell-edge unknowns(auxiliary unknowns) are introduced. When eliminating these cell-edge unknowns by using a weighted combination of their neighboring cell-centered unknowns, we no longer require the weighted coefficient to be nonnegative, but just require the approximation to have second-order accuracy. This idea allows our scheme to adapt to solving the diffusion problem with discontinuous coefficient on universal distorted meshes. Second, the conservative flux is constructed by using a nonlinear weighted combination of these two one-sided edge linear fluxes. Due to the appearance of negative weighted coefficients in the first step, the scheme does not preserve the DMP so far. Then, we come up with a new nonlinear method to transform the conservative flux into a new one which possesses the structure of preserving the DMP. This is one of the key ideas of our work.

The remainder of this article is organized as follows. In Section 2, the construction of the nonlinear

finite volume scheme is described. In Section 3, a prior estimation and the proof preserving the DMP of our scheme are proposed. In Section 4, some numerical results are presented to test the accuracy and verify the DMP. Finally, some conclusions are given.

2. Construction of scheme

Consider the following stationary diffusion problem:

$$-\nabla \cdot (\kappa \nabla u) = f \qquad in \quad \Omega, \tag{2.1}$$

$$u(x) = g \qquad on \quad \partial\Omega, \tag{2.2}$$

where the diffusion tensor κ is a positive-definite matrix, $f \in L^2(\Omega)$, and $g \in C(\partial\Omega)$ are given functions. Let Ω be an open bounded polygonal domain in R^2 with boundary $\partial\Omega$.

2.1. The one-side edge flux

In this subsection, we present the expression of the one-side edge flux with both cell-center unknowns and cell-edge unknowns. Denote the cell by K or L, which also stand for the cell-center, and $\sigma = K|L$ is the common cell-edge of cell K and L. Then, integrate (2.1) over the cell K to get

$$\sum_{\sigma \in \mathcal{E}_K} \mathcal{F}_{K,\sigma} = \int_K f(x) d\mathbf{x}, \tag{2.3}$$

where $\mathcal{E}_K$ is the set of all cell-edges of K and $\mathcal{F}_{K,\sigma}$ is the continuous flux on the edge σ whose expression is as follows:

$$\mathcal{F}_{K,\sigma} = -\int_\sigma \nabla u(x) \cdot \kappa(x)^T \mathbf{n}_{K\sigma} dl. \tag{2.4}$$

The unit outer normal vector on the edge σ of cell K(resp.L) is denoted by $\mathbf{n}_{K\sigma}$(resp.$\mathbf{n}_{L\sigma}$), and the unit tangential vector on the line KM_i(resp.LM_i)$(i = 1, 2)$ is denoted by $\mathbf{t}_{KM_i}$(resp.$\mathbf{t}_{LM_i}$). These notations are shown in Figure 1.

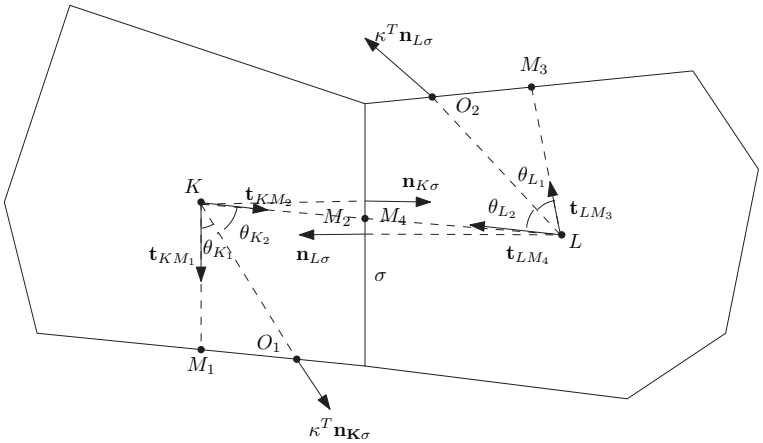

Figure 1. Notations.

Since KM_1 and KM_2 are two edges of triangle KM_1M_2, the two vectors $\mathbf{t}_{KM_1}$ and $\mathbf{t}_{KM_2}$ cannot be collinear (see Figure 1). Then, there is

$$\frac{\kappa^T\mathbf{n}_{K\sigma}}{|\kappa^T\mathbf{n}_{K\sigma}|} = \frac{sin\theta_{K_2}}{sin\theta_K}\mathbf{t}_{KM_1} + \frac{sin\theta_{K_1}}{sin\theta_K}\mathbf{t}_{KM_2}. \tag{2.5}$$

Similarly, there is

$$\frac{\kappa^T\mathbf{n}_{L\sigma}}{|\kappa^T\mathbf{n}_{L\sigma}|} = \frac{sin\theta_{L_2}}{sin\theta_L}\mathbf{t}_{LM_3} + \frac{sin\theta_{L_1}}{sin\theta_L}\mathbf{t}_{LM_4}. \tag{2.6}$$

Substituting (2.5) and (2.6) into (2.4), respectively, we obtain

$$\begin{aligned}\mathcal{F}_{K,\sigma} &= -\int_\sigma |\kappa^T\mathbf{n}_{K\sigma}|\Big(\frac{sin\theta_{K_2}}{sin\theta_K}\nabla u(x)\cdot\mathbf{t}_{KM_1} + \frac{sin\theta_{K_1}}{sin\theta_K}\nabla u(x)\cdot\mathbf{t}_{KM_2}\Big)dl\\ &= -|\kappa^T(K)\mathbf{n}_{K\sigma}||\sigma|\Big(\frac{sin\theta_{K_2}}{sin\theta_K}\frac{u(M_1)-u(K)}{|KM_1|} + \frac{sin\theta_{K_1}}{sin\theta_K}\frac{u(M_2)-u(K)}{|KM_2|}\Big) + O(h^2),\end{aligned}$$

$$\begin{aligned}\mathcal{F}_{L,\sigma} &= -\int_\sigma |\kappa^T\mathbf{n}_{L\sigma}|\Big(\frac{sin\theta_{L_2}}{sin\theta_L}\nabla u(x)\cdot\mathbf{t}_{LM_3} + \frac{sin\theta_{L_1}}{sin\theta_L}\nabla u(x)\cdot\mathbf{t}_{LM_4}\Big)dl\\ &= -|\kappa^T(L)\mathbf{n}_{L\sigma}||\sigma|\Big(\frac{sin\theta_{L_2}}{sin\theta_L}\frac{u(M_3)-u(L)}{|LM_3|} + \frac{sin\theta_{L_1}}{sin\theta_L}\frac{u(M_4)-u(L)}{|LM_4|}\Big) + O(h^2),\end{aligned}$$

where $h = \Big(\sup_{K\in\mathcal{T}} m(K)\Big)^{\frac{1}{2}}$ and $m(K)$ is the area of cell K. Let

$$F_1 = -|\kappa^T(K)\mathbf{n}_{K\sigma}||\sigma|\Big(\frac{sin\theta_{K_2}}{sin\theta_K}\frac{u_{M_1}-u_K}{|KM_1|} + \frac{sin\theta_{K_1}}{sin\theta_K}\frac{u_{M_2}-u_K}{|KM_2|}\Big), \tag{2.7}$$

$$F_2 = -|\kappa^T(L)\mathbf{n}_{L\sigma}||\sigma|\Big(\frac{sin\theta_{L_2}}{sin\theta_L}\frac{u_{M_3}-u_L}{|LM_3|} + \frac{sin\theta_{L_1}}{sin\theta_L}\frac{u_{M_4}-u_L}{|LM_4|}\Big). \tag{2.8}$$

The above two expressions (2.7) and (2.8) contain the cell-edge unknowns, which are auxiliary unknowns in this scheme. Then, we will eliminate those cell-edge unknowns. According to experience, those cell-edge unknowns can be locally approximated by some neighboring cell-center unknowns. Therefore, the approximation expression of cell-edge unknowns u_{M_i} can be usually written as

$$u_{M_i} = \sum_{j=1}^{J_{M_i,n}} \omega_{M_i,j}u_{K_{M_i,j}}, \tag{2.9}$$

where $u_{K_{M_i,j}}$ are some cell-center unknowns, $\omega_{M_i,j}$ are some corresponding coefficients and $J_{M_i,n}$ is the number of cell-center unknowns involved in the approximation of u_{M_i}. The method for selecting the interpolation mainly depends on two aspects in this scheme. On the one hand, the approximation order is required to be second order to preserve the accuracy of the scheme, which is relatively easier to achieve. On the other hand, the interpolation coefficients are allowed to be negative to enable the scheme to be applied to diffusion equations with anisotropic and discontinuous diffusion coefficients on

any arbitrary distorted mesh. As is well-known, it is a challenge to realize this goal when constructing a scheme preserving the DMP.

Rewrite the expression (2.7) to

$$F_1 = \bar{F}_1 + a_K(u_K - u_L), \tag{2.10}$$

where $\bar{F}_1$ dose not include the term u_L, and a_K is a constant which is negative or nonnegative. Similarly, the expression (2.8) can be rewritten to

$$F_2 = \bar{F}_2 + a_L(u_L - u_K), \tag{2.11}$$

where $\bar{F}_2$ dose not include the term u_K, and a_L is a constant which is negative or nonnegative like a_K.

Set a_σ=min$\{|a_K|, |a_L|\}$, which is a nonnegative constant, and we can rewrite (2.10) and (2.11) to be

$$F_1 = \hat{F}_1 + a_\sigma(u_K - u_L), \tag{2.12}$$

$$F_2 = \hat{F}_2 + a_\sigma(u_L - u_K). \tag{2.13}$$

Therefore,the flux $\mathcal{F}_{K,\sigma}$ and $\mathcal{F}_{L,\sigma}$ can be rewritten as follows:

$$\mathcal{F}_{K,\sigma} = a_\sigma(u_K - u_L) + \hat{F}_1 + O(h^2),$$

$$\mathcal{F}_{L,\sigma} = a_\sigma(u_L - u_K) + \hat{F}_2 + O(h^2).$$

2.2. The definition of conservative flux

If $|\hat{F}_1| \le \varepsilon_1$ and $|\hat{F}_2| \le \varepsilon_1$, where ε_1 is a sufficiently small positive constant, $\varepsilon_1 < Ch^2$, and the flux $\mathcal{F}_{K,\sigma}$ and $\mathcal{F}_{L,\sigma}$ can be rewritten to be

$$\mathcal{F}_{K,\sigma} = a_\sigma(u_K - u_L) + O(h^2),$$

$$\mathcal{F}_{L,\sigma} = a_\sigma(u_L - u_K) + O(h^2).$$

Hence, the conservative flux can be easily obtained as follows:

$$F_{K,\sigma} = a_\sigma(u_K - u_L), \tag{2.14}$$

$$F_{L,\sigma} = a_\sigma(u_L - u_K). \tag{2.15}$$

If $|\hat{F}_1| > \varepsilon_1$ or $|\hat{F}_2| > \varepsilon_1$, the construction of the conservative flux becomes complicated. We will make a discussion in this case. Let the discrete flux on edge σ to be

$$F_{K,\sigma} = \lambda_1\hat{F}_1 - \lambda_2\hat{F}_2 + a_\sigma(u_K - u_L), \tag{2.16}$$

$$F_{L,\sigma} = \lambda_2\hat{F}_2 - \lambda_1\hat{F}_1 + a_\sigma(u_L - u_K), \tag{2.17}$$

where λ_1 and λ_2 are some positive coefficients satisfying $\lambda_1 + \lambda_2 = 1$, which will be determined later. It is obvious that there is $F_{K,\sigma} + F_{L,\sigma} = 0$, which means that the discrete flux on the cell edge σ is surely conservative.

Furthermore, there is $|\hat{F}_1| + |\hat{F}_2| \neq 0$ under the circumstances. Then, we can take

$$\lambda_1 = \frac{|\hat{F}_2|}{|\hat{F}_1| + |\hat{F}_2|}, \qquad \lambda_2 = \frac{|\hat{F}_1|}{|\hat{F}_1| + |\hat{F}_2|}.$$

Hence, the positive coefficients λ_1 and λ_2 have been obtained.

If $\hat{F}_1\hat{F}_2 < 0$, that is, $|\hat{F}_1|\hat{F}_2 = -|\hat{F}_2|\hat{F}_1$, then, Eqs (2.16) and (2.17) can be rewritten as follows:

$$\begin{aligned} F_{K,\sigma} =& \frac{|\hat{F}_2|}{|\hat{F}_1| + |\hat{F}_2|}\hat{F}_1 - \frac{|\hat{F}_1|}{|\hat{F}_1| + |\hat{F}_2|}\hat{F}_2 + a_\sigma(u_K - u_L) \\ =& \frac{2|\hat{F}_2|}{|\hat{F}_1| + |\hat{F}_2|}\hat{F}_1 + a_\sigma(u_K - u_L) \\ =& 2\lambda_1\hat{F}_1 + a_\sigma(u_K - u_L), \end{aligned} \tag{2.18}$$

$$\begin{aligned} F_{L,\sigma} =& \frac{|\hat{F}_1|}{|\hat{F}_1| + |\hat{F}_2|}\hat{F}_2 - \frac{|\hat{F}_2|}{|\hat{F}_1| + |\hat{F}_2|}\hat{F}_1 + a_\sigma(u_L - u_K) \\ =& \frac{2|\hat{F}_1|}{|\hat{F}_1| + |\hat{F}_2|}\hat{F}_2 + a_\sigma(u_L - u_K) \\ =& 2\lambda_2\hat{F}_2 + a_\sigma(u_L - u_K). \end{aligned} \tag{2.19}$$

When eliminating those cell-edge unknowns, the appearance of negative coefficients in (2.9) can potentially lead to negative coefficients in $2\lambda_1\hat{F}_1$ of (2.18). However, nonnegative coefficients are crucial for constructing a scheme that satisfes the DMP. To solve this problem, we present a nonlinear correction to the expression of the conservative flux. Let

$$\begin{aligned} u_{K_1} &= \min_{\bar{K}\in\mathcal{J}_K} u_{\bar{K}}, \\ u_{K_2} &= \max_{\bar{K}\in\mathcal{J}_K} u_{\bar{K}}, \end{aligned}$$

where $\mathcal{J}_K$ is the set of all cells which share any vertex with the cell K.

Case1: There exist two cell-centered unknowns $u_{K'}$ and $u_{L'}$ such that

$$\hat{F}_1(u_K - u_{K'}) > 0, \tag{2.20}$$

$$\hat{F}_2(u_L - u_{L'}) > 0, \tag{2.21}$$

where $K' \in \mathcal{J}_K$ and $L' \in \mathcal{J}_L$. In reality, $u_{K'}$ can be taken to be u_{K_1} or u_{K_2}, depending on the circumstances. Similarly, $u_{L'}$ can be treated in the same way.

Therefore, we can rewrite the Eqs (2.18) and (2.19) to be as follows:

$$F_{K,\sigma} = 2\lambda_1\eta_1(u_K - u_{K'}) + a_\sigma(u_K - u_L), \tag{2.22}$$

$$F_{L,\sigma} = 2\lambda_2\eta_2(u_L - u_{L'}) + a_\sigma(u_L - u_K), \tag{2.23}$$

where

$$\eta_1 = \frac{\hat{F}_1}{u_K - u_{K'}},$$

$$\eta_2 = \frac{\hat{F}_2}{u_L - u_{L'}}.$$

According to (2.20), we can see that there is

$$2\lambda_1\eta_1 > 0.$$

Similarly, there is

$$2\lambda_2\eta_2 > 0.$$

Case2: There does not exist two cells $K^{'}$ and $L^{'}$ such that both Eqs (2.20) and (2.21) hold simultaneously. That is,

$$\hat{F}_1(u_K - u_{K'}) \leq 0 \tag{2.24}$$

for any $K^{'} \in \mathcal{J}_K$, or

$$\hat{F}_2(u_L - u_{L'}) \leq 0 \tag{2.25}$$

for any $L^{'} \in \mathcal{J}_L$.

Therefore, we give the following conservative flux,

$$F_{K,\sigma} = a_\sigma(u_K - u_L), \tag{2.26}$$

$$F_{L,\sigma} = a_\sigma(u_L - u_K), \tag{2.27}$$

If $\hat{F}_1\hat{F}_2 \geq 0$, that is, $|\hat{F}_1|\hat{F}_2 = |\hat{F}_2|\hat{F}_1$,then, the Eqs (2.16) and (2.17) can be rewritten as follows:

$$F_{K,\sigma} = a_\sigma(u_K - u_L), \tag{2.28}$$

$$F_{L,\sigma} = a_\sigma(u_L - u_K). \tag{2.29}$$

When $\sigma \in \partial\Omega$, we can give the following expression of flux:

$$F_{K,\sigma} = \sum_i a_{K,i}(u_K - u_{K,i}) + \sum_j a_{M,j}(u_K - u_{M,j}),$$

where $u_{K,i}$ are cell-center unknowns associated with cell K and $u_{M,j}$ are cell-edge unknowns located on the boundary $\partial\Omega$ related to cell K.

2.3. The finite volume scheme

The finite volume scheme is as follows:

$$\sum_{\sigma\in\mathcal{E}_K} F_{K,\sigma} = f_K m(K), \qquad \forall K \in \mathcal{P}_{in}, \tag{2.30}$$

$$u_K = g_K, \qquad \forall K \in \mathcal{P}_{out}, \tag{2.31}$$

where $\mathcal{P}_{in}$ is the set of all cell centers which are in the domain Ω and $\mathcal{P}_{out}$ is the set of all midpoints of boundary edge.

Obviously, the scheme results in a nonlinear system. We solve it by using the Picard iteration, and we linearize the flux as follows:

(i) when $|\hat{F}_1| \le \varepsilon_1$ and $|\hat{F}_2| \le \varepsilon_1$,

$$\begin{aligned} F^{(s)}_{K,\sigma} &= a_\sigma(u^{(s)}_K - u^{(s)}_L), \\ F^{(s)}_{L,\sigma} &= a_\sigma(u^{(s)}_L - u^{(s)}_K). \end{aligned}$$

(ii) when $|\hat{F}_1| > \varepsilon_1$ or $|\hat{F}_2| > \varepsilon_1$, $\hat{F}_1\hat{F}_2 < 0$ for Case 1,

$$\begin{aligned} F^{(s)}_{K,\sigma} =& a_\sigma(u^{(s)}_K - u^{(s)}_L) + 2\lambda^{(s-1)}_1 \frac{\hat{F}_1^{(s-1)}}{u^{(s-1)}_K - u^{(s-1)}_{K'}}(u^{(s)}_K - u^{(s)}_{K'}) \\ =& a_\sigma(u^{(s)}_K - u^{(s)}_L) + 2\lambda^{(s-1)}_1 \eta^{(s-1)}_1 (u^{(s)}_K - u^{(s)}_{K'}), \\ F^{(s)}_{L,\sigma} =& a_\sigma(u^{(s)}_L - u^{(s)}_K) + 2\lambda^{(s-1)}_2 \frac{\hat{F}_2^{(s-1)}}{u^{(s-1)}_L - u^{(s-1)}_{L'}}(u^{(s)}_L - u^{(s)}_{L'}) \\ =& a_\sigma(u^{(s)}_L - u^{(s)}_K) + 2\lambda^{(s-1)}_2 \eta^{(s-1)}_2 (u^{(s)}_L - u^{(s)}_{L'}). \end{aligned}$$

(iii) when $|\hat{F}_1| > \varepsilon_1$ or $|\hat{F}_2| > \varepsilon_1$, $\hat{F}_1\hat{F}_2 < 0$ for Case 2,

$$\begin{aligned} F^{(s)}_{K,\sigma} &= a_\sigma(u^{(s)}_K - u^{(s)}_L), \\ F^{(s)}_{L,\sigma} &= a_\sigma(u^{(s)}_L - u^{(s)}_K). \end{aligned}$$

(iv) when $|\hat{F}_1| > \varepsilon_1$ or $|\hat{F}_2| > \varepsilon_1$, $\hat{F}_1\hat{F}_2 \ge 0$,

$$\begin{aligned} F^{(s)}_{K,\sigma} &= a_\sigma(u^{(s)}_K - u^{(s)}_L), \\ F^{(s)}_{L,\sigma} &= a_\sigma(u^{(s)}_L - u^{(s)}_K). \end{aligned}$$

Here, s is the nonlinear iteration index.

Let $A(U)$ be the matrix of this system, where U is the vector of discrete unknowns. The global discrete nonlinear system reads as:

$$A(U)U = B. \tag{2.32}$$

We choose a small value $\varepsilon_{non} > 0$ and initial vector U^0 in the Picard iteration, and repeat for $s = 1, 2, \ldots,$

1) solve $A(U^{s-1})U^s = B$,

2) stop if $\|A(U^s)U^s - B\| \le \varepsilon_{non}$.

In this paper, we take $\varepsilon_{non} = 10^{-5}$.

3. Analysis

In this section, we give the prior estimation and analysis of maximum principle. Let $\mathcal{E}$ be the set of all cell-edges. Define the norms

$$\|v\|_{L^2} = (\sum_{K\in\mathcal{J}} v_K^2 m(K))^{1/2}, \|\nabla v\| = (\sum_{\sigma\in\mathcal{E}} (v_K - v_L)^2)^{1/2}.$$

Before giving the prior estimation, we need to give the assumption (**H1**) that the scheme (2.30) and (2.31) satisfies the coercivity property. That is, the following inequality holds:

$$\sum_{\sigma\in\mathcal{E}} F_{K,\sigma}(u_K - u_L) \geq C_1\|\nabla u\|^2, \tag{3.1}$$

where C_1 is a constant independent of h.

3.1. The prior estimation

For the nonlinear correction scheme in this paper, we can get the priori estimation.

Theorem 1. Under the assumption (**H1**), for any solution u of the scheme (2.30) and (2.31), there holds

$$\|\nabla u\|^2 \leq C_3\|f\|_{L^2}^2,$$

where C_3 is a positive constant independent of h.

Proof. Multiply (2.30) by u_K and sum up these products for all K to obtain

$$\sum_{K\in\mathcal{J}}\sum_{\sigma\in\mathcal{E}_K} F_{K,\sigma}u_K = \sum_{K\in\mathcal{J}} f_K u_K m(K).$$

Noticing the conservation of the normal flux, we can get

$$\sum_{\sigma\in\mathcal{E}} F_{K,\sigma}(u_K - u_L) = \sum_{K\in\mathcal{J}} f_K u_K m(K).$$

Using the assumption (**H1**), we can get the following inequality:

$$\sum_{\sigma\in\mathcal{E}} F_{K,\sigma}(u_K - u_L) \geq C_1\|\nabla u\|^2.$$

Hence, there is

$$\|\nabla u\|^2 \leq \frac{1}{C_1}\Big(\|f\|_{L^2}^2 + \|u\|_{L^2}^2\Big).$$

Using the discrete Poincare inequality,

$$\|u\|_{L^2} \leq C_2\|\nabla u\|$$

We can obtain the inequality as follows:

$$\|\nabla u\|^2 \leq \frac{1}{C_1}\|f\|_{L^2}^2 + \frac{1}{C_1}C_2^2\|\nabla u\|^2.$$

Then, it follows that

$$\|\nabla u\|^2 \leq C_3\|f\|_{L^2}^2.$$

□

3.2. The discrete maximum principle

From the structure of $F_{K,\sigma}$ in Eqs (2.14), (2.22), (2.26) and (2.28), we figure out that the discrete flux has the form:

$$F_{K,\sigma} = \sum_{i=1}^{N_{K,\sigma}} A_{K,\sigma,i}(u_K - u_{K_i}),$$

where $N_{K,\sigma}$ is the number of cell-center unknowns involved in the flux $F_{K,\sigma}$. We can easily know that $A_{K,\sigma,i} \geq 0$. Then, the finite volume scheme (2.30) reads as:

$$\sum_{i=1}^{N_K} A_{K,i}(u_K - u_{K_i}) = f_K m(K),$$

where N_K is the number of cell-center unknowns related to cell K, and $A_{K,i} \geq 0$, which is the sum of some $A_{K,\sigma,i}$. So far, we conclude that our scheme satisfies the DMP.

Theorem 2. The finite volume scheme (2.30) and (2.31) preserves the discrete maximum principle. Let $u_{min} = \min\limits_{K\in\mathcal{P}_{in}\cup\mathcal{P}_{out}} u_K$ and $u_{max} = \max\limits_{K\in\mathcal{P}_{in}\cup\mathcal{P}_{out}} u_K$, then u_{min} and u_{max} are only obtained on the boundary unless u is a constant in the whole domain. That is, u_{min} can be only obtained on the boundary of domain unless u is a constant for $f \geq 0$, and u_{max} can be only obtained on the boundary of domain unless u is a constant for $f \leq 0$.

The proof of this theorem is similar to some existing papers, so we do not prove it any more.

4. Numerical experiment

As usual, we use discrete L_2-norms to evaluate approximate errors. The L_2-norm for the solution u is taken to be $\varepsilon_2^{\mathrm{u}} = \left[\sum_{K\in\mathcal{T}}(\mathrm{u}_K - \mathrm{u}(K))^2 m(K)\right]^{\frac{1}{2}}$ and the L_2-norm for the flux F is taken to be $\varepsilon_2^{\mathrm{F}} = \left[\sum_{K\in\mathcal{T}}(\mathrm{F}_{K,\sigma} - \mathcal{F}_{K,\sigma})^2\right]^{\frac{1}{2}}$.

4.1. Test 1: The linear elliptic equation with continuous coefficients

Test the linear elliptic equation with continuous coefficient in unit square $\Omega = (0,1)^2$. The diffusion coefficient is

$$\kappa = \begin{pmatrix} cos\theta & sin\theta \\ -sin\theta & cos\theta \end{pmatrix}\begin{pmatrix} k_1 & 0 \\ 0 & k_2 \end{pmatrix}\begin{pmatrix} cos\theta & -sin\theta \\ sin\theta & cos\theta \end{pmatrix},$$

where $k_1 = 1 + 2x^2 + y^2$, $k_2 = 1 + x^2 + 2y^2$, and $\theta = \frac{5\pi}{12}$. The exact solution is taken as $u(x,y) = sin(\pi x)sin(\pi y)$.

We apply our scheme and the scheme in [13] to solve this problem on quadrilateral meshes shown in Figure 2 and triangular meshes shown in Figure 3. Tables 1 and 2 exhibit the error and convergence of these two schemes for test 1 on these two kinds of meshes, respectively. From these two tables, it's easy to find that the convergence rate of our new scheme for the solution is almost second-order and the flux is more than first-order. Meanwhile, we discover that the error of the solution of our new

method is similar to the scheme in [13] by this test example, but the accuracy of the flux remarkably reduced for our new scheme compared to the scheme in [13].

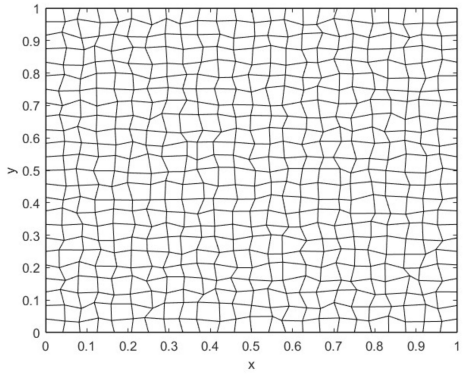

Figure 2. Random quadrilateral meshes.

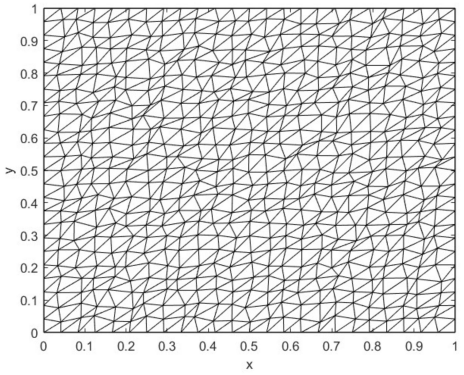

Figure 3. Random triangular meshes.

Table 1. Convergent results of our scheme and scheme in [13] for Test 1 on random quadrilateral meshes.

	number of cells	144	576	2304	9216	36,864
our scheme	$\varepsilon_2^{\mathrm{u}}$	3.71e-3	9.26e-4	2.03e-4	4.87e-5	1.25e-5
	rate	-	2.00	2.19	2.06	1.96
	$\varepsilon_2^{\mathrm{F}}$	4.85e-1	2.22e-1	9.17e-2	3.56e-2	1.33e-2
	rate	-	1.13	1.28	1.37	1.42
scheme in [13]	$\varepsilon_2^{\mathrm{u}}$	3.80e-3	9.33e-4	3.13e-4	5.36e-5	1.37e-5
	rate	-	2.03	1.58	2.54	1.97
	$\varepsilon_2^{\mathrm{F}}$	9.00e-1	4.79e-1	2.13e-1	9.56e-2	4.30e-2
	rate	-	0.91	1.17	1.16	1.15

4.2. Test 2: The linear elliptic equation with discontinuous coefficients

Consider the problem (2.1) and (2.2) with discontinuous coefficients in the unit square $\Omega = (0,1)^2$, where

$$\kappa(x,y) = \begin{cases} 4, & (x,y) \in (0,\frac{2}{3}] \times (0,1), \\ 1, & (x,y) \in (\frac{2}{3},1) \times (0,1), \end{cases}$$

and

$$f(x,y) = \begin{cases} 20\pi^2 \sin \pi x \sin 2\pi y, & (x,y) \in (0,\frac{2}{3}] \times (0,1), \\ 20\pi^2 \sin 4\pi x \sin 2\pi y, & (x,y) \in (\frac{2}{3},1) \times (0,1). \end{cases}$$

The exact solution is

$$\mathrm{u}(x,y) = \begin{cases} \sin \pi x \sin 2\pi y, & (x,y) \in (0,\frac{2}{3}] \times (0,1), \\ \sin 4\pi x \sin 2\pi y, & (x,y) \in (\frac{2}{3},1) \times (0,1). \end{cases}$$

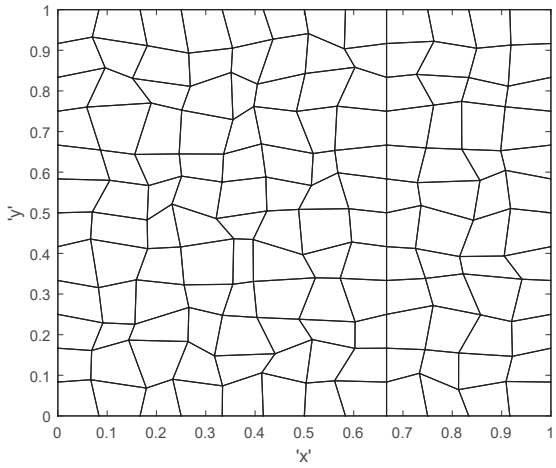

Figure 4. Random quadrilateral meshes with a discontinuity at $x = 2/3$.

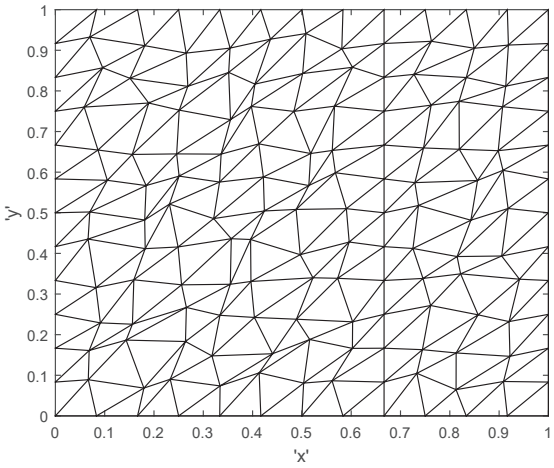

Figure 5. Random triangular meshes with a discontinuity at $x = 2/3$.

Table 2. Convergent results of our scheme and scheme in [13] for Test 1 on random triangular meshes.

	number of cells	288	1152	4608	18,432	73,728
our scheme	$\varepsilon_2^{\mathrm{u}}$	1.44e-2	3.91e-3	1.17e-3	3.04e-4	7.45e-5
	rate	-	1.88	1.74	1.94	2.03
	$\varepsilon_2^{\mathrm{F}}$	1.84e-1	7.53e-2	2.86e-2	1.08e-2	3.91e-3
	rate	-	1.29	1.40	1.41	1.47
scheme in [13]	$\varepsilon_2^{\mathrm{u}}$	1.79e-2	5.87e-3	1.71e-3	4.18e-4	1.06e-4
	rate	-	1.61	1.78	2.03	1.97
	$\varepsilon_2^{\mathrm{F}}$	3.78e-1	1.84e-1	7.63e-2	3.35e-2	1.49e-2
	rate	-	1.03	1.27	1.19	1.17

By using our scheme and the scheme in [13], we test the discontinuous problem on random quadrilateral and triangular meshes with a discontinuity given in Figures 4 and 5. The errors are exhibited in Tables 3 and 4, respectively. We can easily know that our scheme gains nearly second-order accuracy for the solution and more than first-order accuracy for the flux on both kinds of meshes.

From Table 3, we can see that the accuracy of the solution of our scheme reduces a little compared to the scheme in [13], but the accuracy of the flux reduces a lot. From Table 4, the accuracy of the solution and the flux of our new scheme are both remarkably higher than the scheme in [13]. Overall, our new nonlinear scheme is relatively better suited for solving diffusion equations with anisotropic and discontinuous coefficients on distorted meshes.

4.3. Test 3: The linear elliptic equation with linear solution

Consider the problem (2.1) and (2.2) with diffusion coefficients

$$\kappa(x,y) = \begin{cases} 4, & (x,y) \in (0,\frac{2}{3}] \times (0,1) \\ 1, & (x,y) \in (\frac{2}{3},1) \times (0,1), \end{cases}$$

Table 3. Convergent results of our scheme and scheme in [13] for Test 2 with discontinuous coefficient on random quadrilateral meshes.

	number of cells	144	576	2304	9216	36,864
our scheme	$\varepsilon_2^{\mathrm{u}}$	2.65e-2	7.72e-3	2.14e-3	6.04e-4	1.58e-4
	rate	-	1.78	1.85	1.83	1.94
	$\varepsilon_2^{\mathrm{F}}$	3.56e-1	1.97e-1	8.25e-2	3.62e-2	1.63e-2
	rate	-	0.85	1.26	1.19	1.15
scheme in [13]	$\varepsilon_2^{\mathrm{u}}$	2.58e-2	7.42e-3	2.26e-3	6.95e-4	2.02e-4
	rate	-	1.80	1.72	1.70	1.78
	$\varepsilon_2^{\mathrm{F}}$	8.03e-1	4.11e-1	1.78e-1	7.99e-2	3.62e-2
	rate	-	0.97	1.21	1.16	1.14

Table 4. Convergent results of our scheme and scheme in [13] for Test 2 with discontinuous coefficient on random triangular meshes.

	number of cells	288	1152	4608	18,432	73,728
our scheme	$\varepsilon_2^{\mathrm{u}}$	5.15e-2	1.82e-2	4.96e-3	1.31e-3	3.10e-4
	rate	-	1.50	1.88	1.92	2.08
	$\varepsilon_2^{\mathrm{F}}$	1.23	6.71e-1	2.67e-1	1.14e-1	4.79e-2
	rate	-	0.87	1.33	1.23	1.25
scheme in [13]	$\varepsilon_2^{\mathrm{u}}$	7.10e-2	3.03e-2	9.40e-3	2.79e-3	7.10e-4
	rate	-	1.23	1.69	1.75	1.97
	$\varepsilon_2^{\mathrm{F}}$	2.25	1.22	5.13e-1	2.32e-1	1.01e-1
	rate	-	0.88	1.25	1.14	1.20

Table 5. Accuracy for the problem with linear solution on random quadrilateral meshes.

number of cells	144	576	2304	9216
$\varepsilon_2^{\mathrm{u}}$	8.8380e-15	4.6259e-15	2.3390e-15	3.6564e-15
$\varepsilon_2^{\mathrm{F}}$	5.0183e-13	3.1671e-13	5.5543e-13	4.6379e-13

Table 6. Accuracy for the problem with linear solution on random triangle meshes.

number of cells	288	1152	4608	18,432
$\varepsilon_2^{\mathrm{u}}$	1.6754e-14	2.1597e-14	2.6963e-15	5.1886e-15
$\varepsilon_2^{\mathrm{F}}$	1.5465e-12	1.8797e-12	1.2812e-12	2.0331e-12

and source term $f = 0$. Take the following linear solution:

$$\mathrm{u}(x, y) = \begin{cases} 1 + x + y, & (x, y) \in (0, \frac{2}{3}] \times (0, 1) \\ -1 + 4x + y, & (x, y) \in (\frac{2}{3}, 1) \times (0, 1). \end{cases}$$

We set the stopping criterion $\varepsilon_{non} = 10^{-14}$ for this example, and test it on random quadrilateral meshes and random triangular meshes, respectively. Computational results are shown in Tables 5 and 6. Both tables demonstrate that our scheme can accurately recover the linear solution.

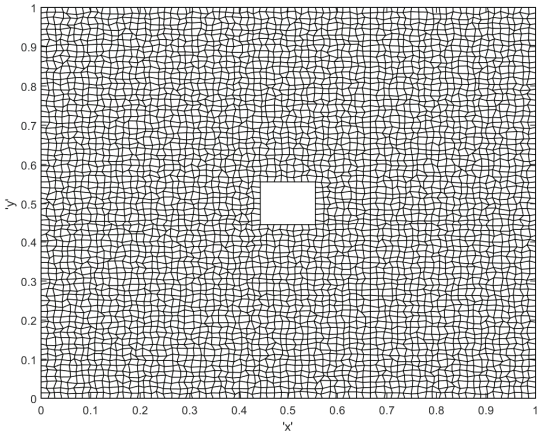

Figure 6. Random quadrilateral meshes with a hole and a discontinuity at $x = 2/3$ (number of cells is 72×72).

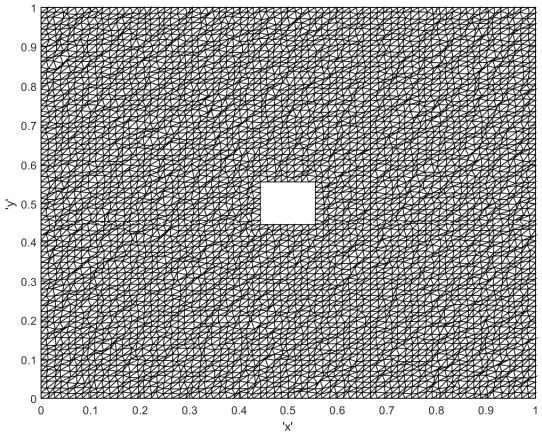

Figure 7. Random triangular meshes with a hole and a discontinuity at $x = 2/3$ (number of cells is $72 \times 72 \times 2$).

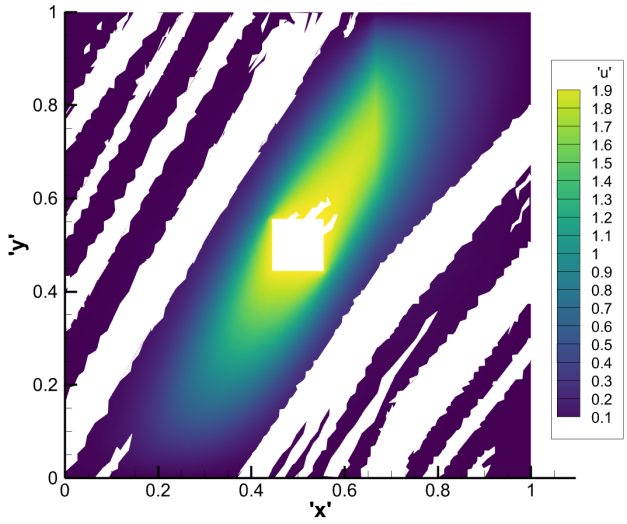

Figure 8. The numerical solution of scheme in [25] on random quadrilateral meshes with a hole and a discontinuity at $x = 2/3$ ($u_{min} = -5.36e-2$, $u_{max} = 2.0847$, the overshoot and undershoot are shown in white).

4.4. Test 4: The linear elliptic equation on the domain with a hole

Consider the problem (2.1) and (2.2) on the domain $\Omega = (0,1)^2 \backslash [4/9, 5/9]^2$, whose boundary $\partial\Omega$ is composed of two disjoint parts Γ_1 and Γ_0 exhibited in Figures 6 and 7, where Γ_1 is the interior boundary and Γ_0 is the exterior boundary. Set $f = 0$, $g = 0$ on Γ_0, and $g = 2$ on Γ_1. Take the anisotropic diffusion tensor κ as follows:

$$\kappa = \begin{pmatrix} cos\theta & sin\theta \\ -sin\theta & cos\theta \end{pmatrix} \begin{pmatrix} k_1 & 0 \\ 0 & k_2 \end{pmatrix} \begin{pmatrix} cos\theta & -sin\theta \\ sin\theta & cos\theta \end{pmatrix},$$

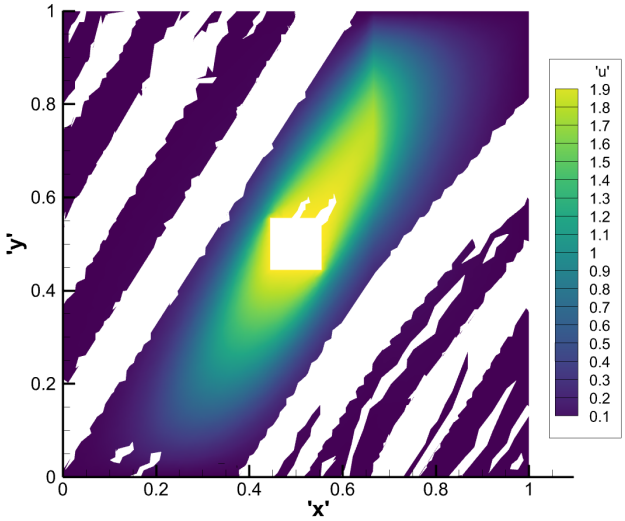

Figure 9. The numerical solution of scheme in [25] on random triangular meshes with a hole and a discontinuity at $x = 2/3$ ($u_{min} = -7.58e-3$, $u_{max} = 2.1016$, the overshoot and undershoot are shown in white).

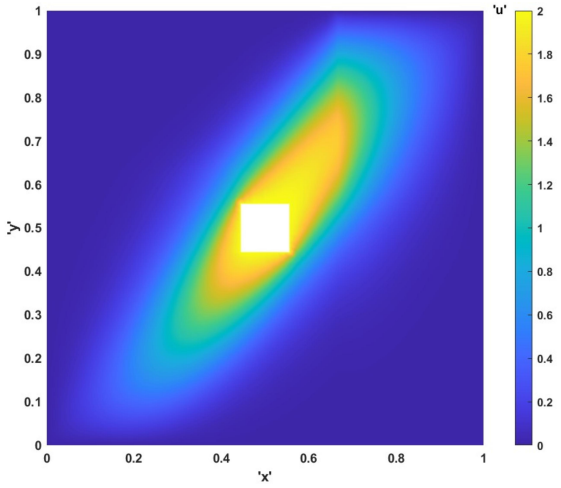

Figure 10. The numerical solution of our new scheme on random quadrilateral meshes with a hole and a discontinuity at $x = 2/3$ ($u_{min} = 0$ and $u_{max} = 2$).

where $k_1 = 1$, $k_2 = \begin{cases} 100, & (x, y) \in (0, \frac{2}{3}] \times (0, 1) \\ 10, & (x, y) \in (\frac{2}{3}, 1) \times (0, 1) \end{cases}$, and $\theta = \frac{\pi}{6}$.

We test this example on random quadrilateral meshes with a hole shown in Figure 6 and random triangular meshes with a hole shown in Figure 7. The contour of the numerical solution of the scheme in [25] on these two kinds of meshes are shown in Figures 8 and 9, respectively. The analysis of both figures reveals that the numerical solution exhibits negative minima and surpasses the value of 2 at its maxima. Consequently, the scheme in [25] violates the DMP.

The numerical solution of our new scheme on these two kinds of meshes are shown in Figures 10

and 11, respectively. Both figures show that the numerical solution maintains a minimum value of 0 and reaches a maximum value of 2. These results testify that our scheme satisfies the DMP.

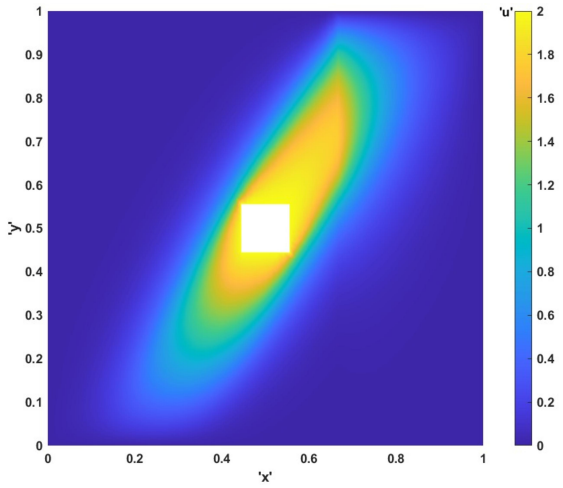

Figure 11. The numerical solution of our new scheme on random triangular meshes with a hole and a discontinuity at $x = 2/3$ ($u_{min} = 0$ and $u_{max} = 2$).

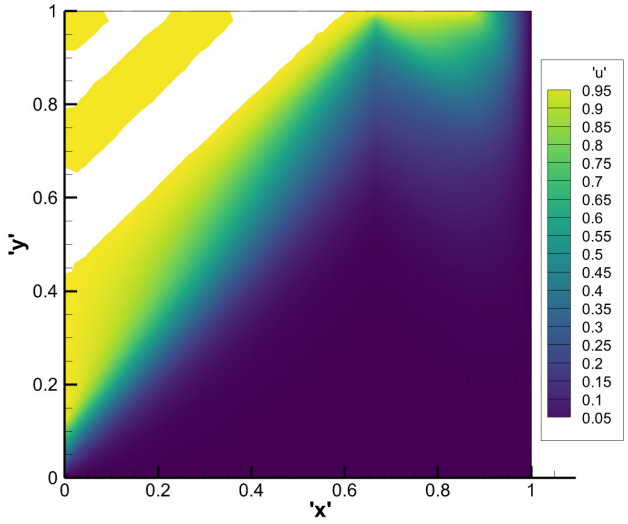

Figure 12. The numerical solution of scheme in [26] on random quadrilateral meshes with a discontinuity at $x = 2/3$ ($u_{min} = 0$, $u_{max} = 1.0120$, the overshoot is shown in white).

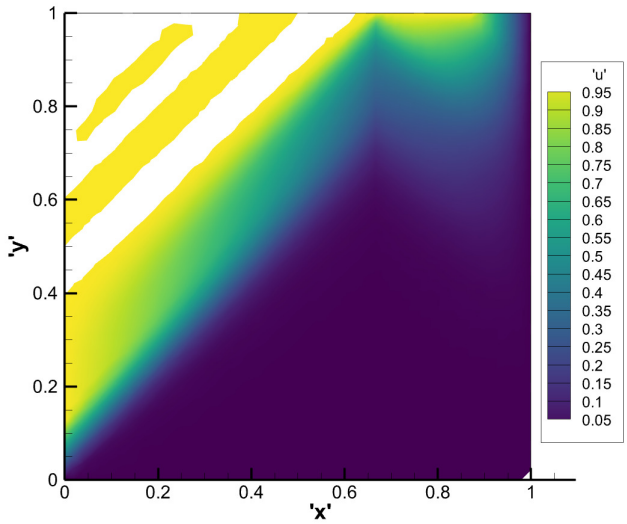

Figure 13. The numerical solution of scheme in [26] on random triangular meshes with a discontinuity at $x = 2/3$ ($u_{min} = 0$, $u_{max} = 1.0063$, the overshoot is shown in white).

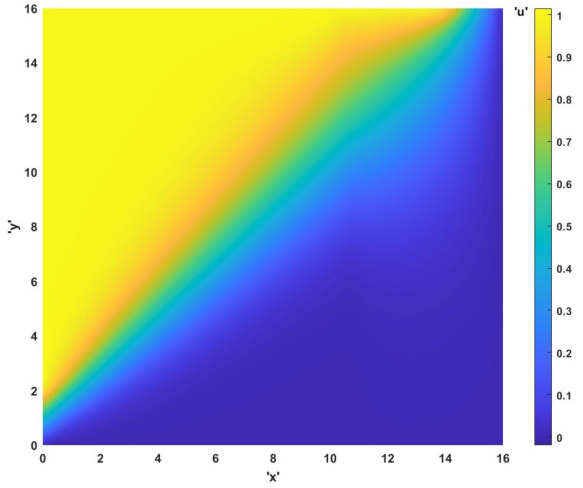

Figure 14. The numerical solution of our scheme on random quadrilateral meshes with a discontinuity at $x = 2/3$ ($u_{min} = 0$ and $u_{max} = 1$).

4.5. Test 5: The linear elliptic equation with anisotropic solution

Consider the problem (2.1) and (2.2) with discontinuous and anisotropic diffusion tensor coefficients as follows:

$$\kappa = \begin{cases} \begin{pmatrix} 500.5 & 499.5 \\ 499.5 & 500.5 \end{pmatrix}, & (x, y) \in (0, \frac{2}{3}] \times (0, 1) \\ \begin{pmatrix} 1/2 & 1/3 \\ 1/3 & 1/2 \end{pmatrix}, & (x, y) \in (\frac{2}{3}, 1) \times (0, 1). \end{cases}$$

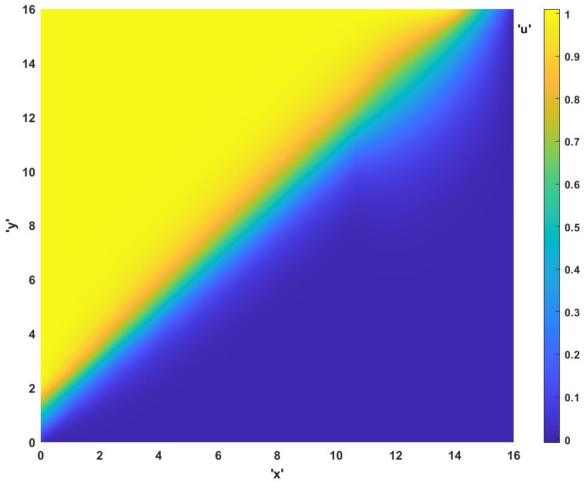

Figure 15. The numerical solution of our scheme on random triangular meshes with a discontinuity at $x = 2/3$ ($u_{min} = 0$ and $u_{max} = 1$).

The computational domain is $\Omega = (0, 16) \times (0, 16)$. We set $f = 0$, $g(x, 0) = 0$, $g(16, y) = 0$,

$$g(0, y) = \begin{cases} 0.5y, & 0 \le y < 2, \\ 1, & 2 \le y \le 16, \end{cases}$$

and

$$g(x, 16) = \begin{cases} 1, & 0 \le x \le 14, \\ 8 - 0.5x, & 14 < x \le 16. \end{cases}$$

Though the solution of the problem is unknown, the maximum principle states that the solution of this problem should stay between 0 and 1.

We first use the positivity-preserving scheme in [26] to test this example on the random quadrilateral meshes with 48×48 cells and the random triangular meshes with $48 \times 48 \times 2$ cells. The contour of the numerical solution on random quadrilateral meshes is shown in Figure 12, and that on random triangular meshes is shown in Figure 13. Both figures reveal that the peak value of the numerical solution surpasses 1. The numerical findings indicate that the positivity-preserving scheme fails to maintain the upper bound constraints of the solution.

We use our nonlinear scheme to test this example on the same two kinds of meshes. Results are presented in Figures 14 and 15, respectively. From these two figures, we see that our new scheme avoids undershoot and overshoot, which testify that our scheme satisfies the DMP.

5. Conclusions

An improved nonlinear finite volume scheme which preserves the DMP for the diffusion problem with anisotropic and discontinuous coefficients is developed. This new scheme can solve diffusion equations with the discontinuous coefficient on any arbitrary distorted meshes, overcoming the drawback of existing schemes that require the interpolation coefficients of cell-edge unknowns to be nonnegative. We provide a prior estimation based on an assumption of the coercivity property. Numerical results demonstrate that the accuracy of this new scheme surpasses that of the existing scheme. Furthermore, numerical results testify that this new scheme satisfies the DMP. When solving the nonlinear

algebraic system, we find that the Picard iteration is unsatisfactory in terms of computational efficiency. We hope to detect a useful iteration method that is adapted for this system in the future.

Use of AI tools declaration

The authors declare they have not used Artificial Intelligence (AI) tools in the creation of this article.

Acknowledgments

This work is partially supported by Shandong Provincial Natural Science Fundation (ZR2021QA109), National Natural Science Foundation of China (No. 12101536) and the LCP Fund for Young Scholar (No. 6142A05QN22004).

Conflict of interest

The authors declare there is no conflicts of interest.

References

1. F. Hermeline, A finite volume method for the approximation of diffusion operators on distorted meshes, *J. Comput. Phys.*, **160** (2000), 481–499. https://doi.org/10.1006/jcph.2000.6466
2. J. M. Nordbotten, I. Aavatsmark, Monotonicity conditons for control volume methods on uniform parallelogram grids in homogeneous media, *Comput. Geosci.*, **9** (2005), 61–72. https://doi.org/10.1007/s10596-005-5665-2
3. E. Bertolazzi, G. Manzini, A second-order maximum principle preserving finite volume method for steady convection-diffusion problems, *SIAM J. Numer. Anal.*, **43** (2005), 2172–2199. https://doi.org/10.1137/040607071
4. J. Droniou, Finite volume schemes for diffusion equations: Introduction to and review of modern methods, *Math. Models Methods Appl. Sci.*, **24** (2014), 1575–1619. https://doi.org/10.1142/S0218202514400041
5. C. L. Potier, Finite volume monotone scheme for highly anisotropic diffusion operators on unstructured triangular meshes, *C. R. Math.*, **341** (2005) 787–792. https://doi.org/10.1016/j.crma.2005.10.010
6. K. Lipnikov. D. Svyatskiy, Y. Vassilevski, Monotone finite volume method for diffusion equations on unstructured triangular and shape-regular polygonal meshes, *J. Comput. Phys.*, **227** (2007), 492–512. https://doi.org/10.1016/j.jcp.2007.08.008
7. Z. Sheng, J. Yue, G. Yuan, Monotone finite volume schemes of nonequilibrium radiation diffusion equations on distorted meshes, *SIAM J. Sci. Comput.*, **31** (2009), 2915–2934. https://doi.org/10.1137/080721558
8. K. Lipnikov, D. Svyatskiy, Y. Vassilevski, A monotone finite volume method for advection-diffusion equations on unstructured polygonal meshes, *J. Comput. Phys.*, **229** (2010), 4017–4032. https://doi.org/10.1016/j.jcp.2010.01.035

9. K. Lipnikov, G. Manzini, D. Svyatskiy, Analysis of the monotonicity condition in the mimetic finite difference method for elliptic problems, *J. Comput. Phys.*, **230** (2011), 2620–2642. https://doi.org/10.1016/j.jcp.2010.12.039

10. J. Camier, F. Hermeline, A monotone nonlinear finite volume method for approximating diffusion operators on general meshes, *Int. J. Numer. Methods Eng.*, **107** (2016), 496–519. https://doi.org/10.1002/nme.5184

11. C. L. Potier, A nonlinear finite volume scheme satisfying maximum and minimum principles for diffusion operators, *Int. J. Finite Vol.*, **2** (2009).

12. Z. Sheng, G. Yuan, The finite volume scheme preserving extremum principle for diffusion equations on polygonal meshes, *J. Comput. Phys.*, **230** (2011), 2588–2604. https://doi.org/10.1016/j.jcp.2010.12.037

13. Z. Sheng, G. Yuan, Construction of nonlinear weighted method for finite volume schemes preserving maximum principle, *SIAM J. Sci. Comput.*, **40** (2018), A607–A628. https://doi.org/10.1137/16m1098000

14. Y. Yu, G. Yuan, Z. Sheng, The finite volume scheme preserving maximum principle for diffusion equations with discontinuous coefficient, *Comput. Math. Appl.*, **79** (2020), 2168–2188. https://doi.org/10.1016/j.camwa.2019.10.012

15. S. Su, J. Wu, A symmetric and coercive finite volume scheme preserving the discrete maximum principle for anisotropic diffusion equations on star-shaped polygonal meshes, *Appl. Numer. Math.*, **198** (2024), 217–235. https://doi.org/10.1016/J.APNUM.2024.01.008

16. J. Droniou, C. L. Potier, Construction and convergence study of schemes preserving the elliptic local maximum principle, *SIAM J. Numer. Anal.*, **49** (2011), 459–490. https://doi.org/10.1137/090770849

17. Z. Sheng, G. Yuan, Analysis of nonlinear scheme preserving maximum principle for anisotropic diffusion equation on distorted meshes, *Sci. China Math.*, **65** (2022), 2379–2396. https://doi.org/10.1007/S11425-021-1931-3

18. S. Korotov, M. Krizek. P. Neittaanmäki, Weakened acute type condition for tetrahedral triangulations and the discrete maximum principle, *Math. Comput.*, **70** (2000), 107–119. https://doi.org/10.1090/s0025-5718-00-01270-9

19. E. Burman, A. Ern, Discrete maximum principle for Galerkin approximatios of the Laplace operator on arbitrary meshes, *C. R. Math.*, **338** (2004), 641–646. https://doi.org/10.1016/j.crma.2004.02.010

20. C. Lu, W. Huang, J. Qiu, Maximum principle in linear finite element approximations of anisotropic diffusion-convection-reaction problems, *Numer. Math.*, **127** (2014), 515–537. https://doi.org/10.1007/s00211-013-0595-8

21. W. Huang, Y. Wang, Discrete maximum principle for the weak Galerkin method for anisotropic diffusion problems, *Commum. Comput. Phys.*, **18** (2015), 65–90. https://doi.org/10.4208/cicp.180914.121214a

22. C. Cances, M. Cathala, C. L. Potier, Monotone corrections for generic cell-centered finite volume approximations of anisotropic diffusion equations, *Numer. Math.*, **125** (2013), 387–417. https://doi.org/10.1007/s00211-013-0545-5

23. H. Yang, B. Yu, Y. Li, Monotonicity correction for second order element finite volume methods of anisotropic diffusion problems, *J. Comput. Phys.*, **449** (2022), 110759. https://doi.org/10.1016/J.JCP.2021.110759

24. Z. Sheng, G. Yuan, A nonlinear scheme preserving maximum principle for heterogeneous anisotropic diffusion equation, *J. Comput. Appl. Math.*, **436** (2024). https://doi.org/10.1016/J.CAM.2023.115438

25. Z. Sheng, G. Yuan, A nine point scheme for the approximation of diffusion operators on distorted quadrilateral meshes, *SIAM J. Sci. Comput.*, **30** (2008), 1341–1361. https://doi.org/10.1137/060665853

26. Z. Sheng, G. Yuan, A new nonlinear finite volume scheme preserving positivity for diffusion equations, *J. Comput. Phys.*, **315** (2016), 182–193. https://doi.org/10.1016/j.jcp.2016.03.053

AIMS Press